pH-Responsive Near-Infrared Emitting Conjugated Polymer Nanoparticles for Cellular Imaging and Controlled-Drug Delivery

Jousheed Pennakalathil,[1,2*] Alp Özgün,[2*] Irem Durmaz,[3] Rengül Cetin-Atalay,[3] Dönüs Tuncel[1,2]

[1]Department of Chemistry, Bilkent University, 06800 Ankara, Turkey
[2]National Nanotechnology Research Center, Institute of Material Science and Nanotechnology, Bilkent University, 06800 Ankara, Turkey
[3]Department of Molecular Biology and Genetics, Bilkent University, 06800 Ankara, Turkey
Correspondence to: D. Tuncel (E-mail: dtuncel@fen.bilkent.edu.tr)

Received 2 September 2014; accepted 28 October 2014; published online 17 November 2014
DOI: 10.1002/pola.27458

ABSTRACT: In this article, pH-responsive near-infrared emitting conjugated polymer nanoparticles (CPNs) are prepared, characterized, and their stabilities are investigated under various conditions. These nanoparticles have capacity to be loaded with water insoluble, anticancer drug, camptothecin (CPT), with around 10% drug loading efficiency. The *in vitro* release studies demonstrate that the release of CPTs from CPNs is pH-dependent such that significantly faster drug release at mildly acidic pH of 5.0 compared with physiological pH 7.4 is observed. Time and dose-dependent *in vitro* cytotoxicity tests of blank and CPT-loaded nanoparticles are performed by real-time cell electronic sensing (RT-CES) assay with hepatocellular carcinoma cells (Huh7). The results indicate that CPNs can be effectively utilized as vehicles for pH-triggered release of anticancer drugs. © 2014 Wiley Periodicals, Inc. J. Polym. Sci., Part A: Polym. Chem. **2015**, *53*, 114–122

KEYWORDS: cellular imaging; conjugated polymers; drug delivery systems; luminescence; nanoparticles; near IR emission; pH-responsive

INTRODUCTION The delivery of drugs by nanoparticle-based systems offers many advantages over conventional methods such as reduced systemic toxicity and enhanced drug efficiency on target could be achieved due to enhanced permeation and retention effect (EPR).[1–3] Moreover, these systems can be designed to include multiple moieties such as active site targeting agents, imaging agents, immune evasion mechanisms, and microenvironment sensors for passive targeting at the cost of increased complexity and convoluted working mechanisms with each added moiety.[4] Especially, polymeric nanoparticles are very appropriate for this purpose as their versatile surface chemistry can easily be adjusted for functionalizing with different moieties.[5–7] Furthermore, their sizes can be tuned for different applications by changing simple parameters in the synthesis procedure. Most polymers tend to be biocompatible and show low toxicity due to their chemical inertness or they can be designed to degrade into harmless compounds in biological media. In addition, the microenvironment sensing properties such as pH sensitivity can be added to these polymers by making simple changes in the polymer structure.[8–11] It is known from the literature that endosomes and tumour microenvironments have relatively acidic pH values. Once the drug-loaded nanoparticles are internalized by the cells, some of the endocytosed drug-loaded nanoparticles begin to hydrolyse under acidic environment in endosomes; this will, in turn, causes the swelling of nanoparticles and simultaneous delivery of drugs into the cytosol.[12]

Real-time biological imaging of the tumour site is one of the most important factors in cancer treatment.[13,14] Moreover, combining therapeutic and imaging agents on a single system provides information about drug biodistribution and pathological processes which helps physicians to make more informed decisions on treatment strategies. To this end, there has been great interest to develop multifunctional nanoparticles which contain fluorescence imaging agents.[15] For this purpose, small fluorescent dyes and fluorescent proteins are used as traditional fluorescent markers but they exhibit poor photostability as they fade away rapidly during imaging and this, in turn, limits their use in long term monitoring of live cells.[16] Luminescent nanoparticles such as quantum dots and dye-loaded silica nanoparticles are found to be suitable for these purposes as these nanoparticles possess high brightness and photostability compared with small fluorescent dyes. However, their cytotoxicity is considered as a serious problem for their *in vivo* applications because of

*Jousheed Pennakalathil and Alp Özgün contributed equally to this work

Additional Supporting Information may be found in the online version of this article.

the presence of toxic heavy metals (e.g. Cd).[17] Dye-loaded silica nanoparticles also present some drawbacks; only limited amount of dyes can be loaded due to π-π interaction between the dye molecules which causes a reduced fluorescent quantum yields.[18]

An emerging alternative is the use of conjugated polymer particles as fluorescent labels because of their high quantum yields, high molar absorptivity, photo stability, and easy synthesis.[19–31] However, there is not much research on the metabolic processes of these nanoparticles. In the *in vivo* studies, the biodistribution profile of these nanoparticles after 72 h postinjection showed uptake in the tumorous tissue as well as liver and the spleen indicating that they could be cleared out from the body through liver.[32] Although the use of conjugated polymer nanoparticles for dual delivery of therapeutic agents and cell imaging offers many advantages, this strategy is largely unexplored and there are few reports relating to this concept.[33–38] For instance, the inherent fluorescence of the conjugated polymers could eliminate the need for an imaging agent in the designed delivery vehicle thus making the system less complicated. There are many examples in the literature on the pH-responsive polymeric nanoparticles designed for the delivery of drugs;[8,9,39] however, to the best of our knowledge, examples are scarce on the drug delivery system which is based on pH-responsive near-infrared emitting conjugated polymer nanoparticles. Recently we have reported on the red emitting pH-responsive conjugated oligomer-based nanoparticles for drug delivery and cellular imaging.[40] Although these conjugated oligomer-based nanoparticles have many interesting features, they emit in the far red region and exhibit relatively low drug-loading efficiency (5.9%) which needs further improvement. In this context, we report here novel, pH-responsive, near-infrared emitting conjugated polymer nanoparticles with higher drug loading efficiency than oligomer-based nanoparticles for cellular imaging and controlled-drug release. These nanoparticles emit in the near-infrared region; have good photostability and low toxicity that are essentials for biological imaging. Near-infrared emission is highly desirable for bioimaging because it will enable high contrast *in vivo* imaging due to the lack of interference from tissue autofluorescence in the NIR window.[41–43] In addition, due to the pH-sensitive pendant groups on the polymer chains, nanoparticles formed from these polymers are sensitive to lower pH levels found in most tumour microenvironments offering a promise for use in chemotherapeutic drug delivery applications.

EXPERIMENTAL

General

All solvents and reagents including, 2-(thiophen-3-yl)ethanol, 2,1,3-benzothiadiazole-4,7-*bis*(boronic acid pinacol ester), *N*-bromosuccinimide, tetrabutylammonium bromide, bromobenzene, tetrakis(triphenylphosphine)palladium, were purchased from Sigma-Aldrich Chemical Co. and were used as received. ^{1}H and ^{13}C NMR spectra recorded on a Bruker Avance III 400 MHz spectrometer using $CDCl_3$ as a solvent. FT-IR measurements recorded on a Bruker TENSOR 27. Samples were prepared as a KBr pellet. For optical characterization, a UV–Vis spectrophotometer (Cary UV–Vis) and a fluorescence spectrophotometer (Cary Eclipse Fluorescent spectrophotometer) equipped with a xenon-lamp as the excitation source were used. The molecular weight of the polymer P1 was determined using gel permeation chromatography (GPC) on Polymer Laboratories PL-GPC220 system equipped with a RI detector in THF using a calibration curve of polystyrene standards.

Nanoparticles sizes were measured by dynamic light scattering (DLS, Zetasizer Nano-ZS). Measurements were carried out at 633 nm and the laser, as a light source, was used at room temperature. Morphological characterization was done by scanning electron microscopy (SEM, Quanta 200 FEG SEM) and transmission electron microscopy (TEM, FEI Tecnai G2 F30). The DLS measurements were usually repeated at least three times and the average values were reported.

2-(2,5-Dibromothiophen-3-yl)ethyl acetate (M2)

2-(2,5-dibromothiophen-3-yl)ethanol (M1) was synthesized according to literature procedure.[22] A stirred solution of M1 (1.00 g, 3.50 mmol) in 10 mL acetic anhydride was added pyridine (400 μL, 5.24 mmol,) and the reaction mixture was allowed to stir at room temperature for overnight. After the reaction was over, the mixture was diluted with DCM; water was added and the extraction was carried out. Organic phase was collected and washed with water several times. The solvent was evaporated under reduced pressure which provided pale yellow liquid. This was further stirred with 20 mL MeOH for 20 min to convert the remaining acid-anhydride into methylester which was easily evaporated under reduced pressure. Product was purified by Si-gel column chromatography using cyclohexane as an eluent (1.04 g, 90%).

^{1}H-NMR (400 MHz, $CDCl_3$, 25 °C): δ 6.85 (s, 1H, c), 4.25 (t, $^3J = 6.4$ Hz, 2H, a), 2.82 (t, $^3J = 6.4$ Hz, 2H, b), 2.05 (s, 3H, d); ^{13}C-NMR (100 MHz, $CDCl_3$, 25 °C): δ 20.9, 28.9, 62.9, 109.7, 110.9, 131.0, 138.3, 170.7. HRMS (ESI) calcd. for $[M+K\text{-}2H]^-$ ($C_8H_6Br_2KO_2S$) 362.8087, found 362.8006.

Synthesis of Poly [2-(2,5-dibromo-thiophen-3-yl)-ethyl acetate)-co-4,7-(2,1,3-benzothiadiazole)] (P1)

2-(2,5-dibromo-thiophen-3-yl)-ethyl acetate (515.4 mg, 1.581 mmol) and 2,1,3-benzothiadiazole-4,7-*bis*(boronic acid pinacol ester) (613.9 mg, 1.581 mmol) were placed into a two-necked RBF. The mixture was left under vacuum for 20 min. Degassed THF (20 mL) was added and stirred for 10 min. Then the aqueous solution of K_2CO_3 (1500 mg, 7.905 mmol) in 10 mL degassed water was added, TBAB (50 mg) was added and the reaction was stirred for 10 min. Then the mixture was degassed via two cycles of freeze-pump-thaw and the flask was filled with N_2 gas. $Pd(PPh_3)_4$ (91 mg, 0.079 mmol) was added quickly. The mixture was heated to 80 °C under N_2 gas 16 h. Twenty milliliters degassed THF and 10 mL degassed toluene were added. The mixture was

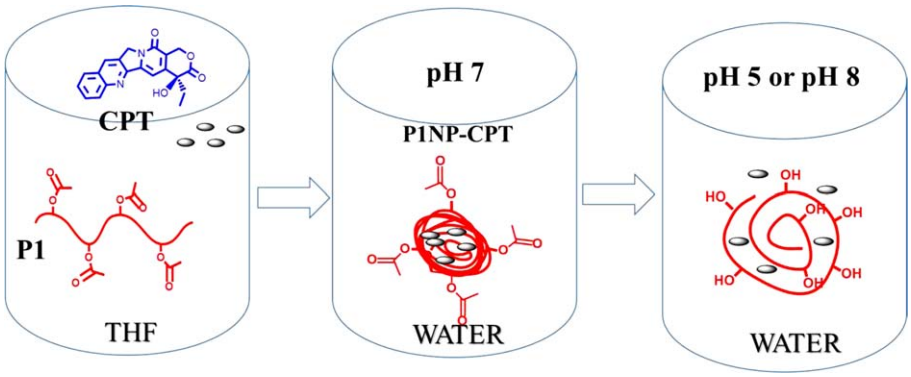

SCHEME 1 An overview of the preparation of drug-loaded nanoparticles and pH-triggered drug release mechanism of the nanoparticles. [Color figure can be viewed in the online issue, which is available at wileyonlinelibrary.com.]

further stirred under N_2. A purple colour solution was obtained. After about 66 h bromobenzene (100 μL) was added and the reaction was further heated 4 h more. After the completion of the reaction, the solvents were removed under reduced pressure and the residue was washed with water several times. Then the precipitate was filtered, washed with MeOH. The crude product was redissolved in THF and precipitated into cold MeOH for further purification. Purple coloured powder was collected and dried under vacuum for 5 h (525 mg, 46%).

^{1}H-NMR (400 MHz, $CDCl_3$, 25 °C): δ: 2.05 (m, 3H), 3.15 (m, 2H), 4.4 (m, 2H), 7.1 (m, 1H), 7.9–8.2 (m, 2H); ^{13}C-NMR (100 MHz, $CDCl_3$, 25 °C): δ 21.0, 29.1, 29.9, 64.2, 125.2, 125.6, 130.1, 130.4, 152.3, 152.6, 170.9.

GPC: $M_n = 2.5 \times 10^4$ g mol^{-1}, $M_w = 5.2 \times 10^4$ g mol^{-1} (THF as a solvent and polystyrene as standard).

Preparation of Nanoparticles of P1

In a typical procedure, P1 (1.0 mg, 3.3×10^{-3} mmol, based on per repeating unit) was dissolved in dry THF (1 mL). The solution was sonicated for ~15 min and then injected rapidly to 20 mL of DD water. The sonication was continued for a further 30 min. THF was removed from the solution under reduced pressure.

RESULTS AND DISCUSSION

Synthesis and Characterization of Polymer P1

For the preparation of pH-responsive and near-infrared emitting nanoparticles, polymer 1 (Scheme 2) (P1) was designed by taking the following points into consideration: P1 is hydrophobic at neutral pH but can be made hydrophilic at low and high pH values by hydrolysing the acetyl groups to hydrophilic hydroxyl groups. Thus, it would be easier to form nanoparticles and drug-loaded nanoparticles from hydrophobic polymer P1; since the nanoparticles will have more compact shapes at neutral pH and hold the drugs tightly but at low or high pH values due to hydrolysis, the nanoparticles will swell and the polymer chains will be loosely folded because of the interaction of hydroxyl groups with water. This, in turn, will trigger the release of drugs from the nanoparticles (Scheme 1). Besides, P1 itself is self-luminescent and emits in the near infrared region of the spectrum.

This feature offers several advantages such as eliminating the need for an extra fluorophore in the system for cellular imaging and the drugs will be encapsulated in high loading rate because of the favourable interactions with polymer aromatic backbone.

Polymer 1 was synthesized according to the reaction Scheme 2. First 2-(thiophen-3-yl)ethanol was brominated using *N*-bromosuccinimide in ethyl acetate to obtain 2-(2,5-dibromothiophen-3-yl)ethanol[18d] (M1) and then its hydroxyl group was acetylated using acetic acid anhydride to yield the target monomer (M2). Suzuki Coupling of M2 and 1,2,3-benzothiadiazole-4,7-*bis*(boronic acid pinocol ester) afforded polymer P1 in 46% yield as purple powders.

Structural characterization of polymer was carried out via ^{1}H and ^{13}C NMR (Supporting Information Fig. S3) and FT-IR

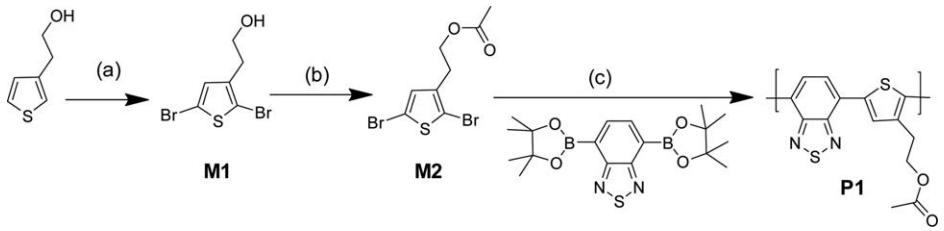

SCHEME 2 Reaction scheme for P1. (a) 2-(thiophen-3-yl)ethanol, NBS, EtOAc, 25 °C, 12 h, 60%; (b) acetic anhydride, pyridine, 25 °C, 12 h, 90%; (c) THF/toluene/H_2O (1:1:1, v/v), K_2CO_3 (aq.), TBAB, $Pd(PPh_3)_4$, 80 °C, 72 h, 46%.

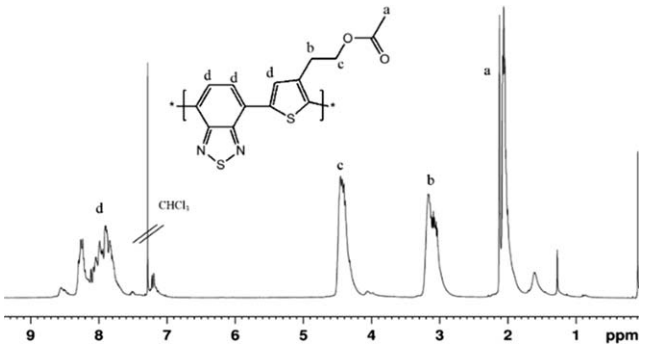

FIGURE 1 ^{1}H-NMR (400 MHz, $CDCl_3$, 25 °C) spectrum of P1.

spectroscopies. Figure 1 show the ^{1}H-NMR spectrum of P1 which confirms the expected structures of the polymer. In the FT-IR spectrum of P1 (Supporting Information Fig. S5), the presence of the characteristic carbonyl stretching at around 1700 cm^{-1} supports further the expected structure of the polymer.

The molecular weight of polymer was determined by GPC (Supporting Information Fig. S6). M_n and M_w values of P1 have been found to be as 25 kDa and 52 kDa, respectively, with polydispersity index (PDI) of 2.1 which is in an expected range for a step-growth polymerization.

Synthesis of Nanoparticles and Investigation of their Stabilities

Nanoparticles were prepared by a simple reprecipitation method as reported in the literature.[37] Briefly, polymer solution in THF is injected into a large excess of water under sonication and by the removal of the THF under reduced pressure, stable nanoparticles are obtained. It is possible to tune the sizes of nanoparticles by varying the concentration of polymers used. Here we used different concentrations of polymer to demonstrate the effect of polymer concentrations on the nanoparticle sizes. The results confirm that the structures and the concentrations of the polymers directly affect the size of nanoparticles; an increase in the polymer concentration causes an increase in the size of the nanoparticles.

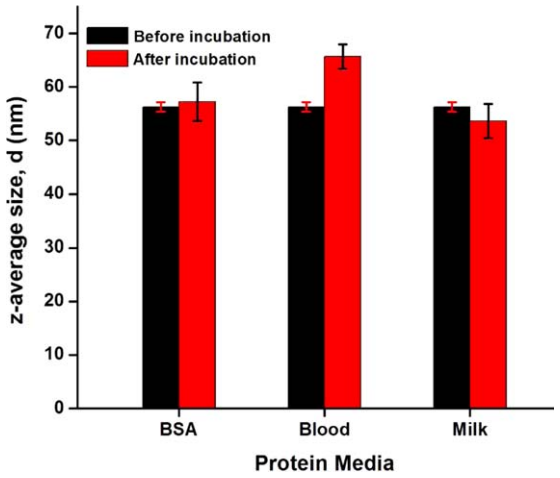

FIGURE 3 The nanoparticles in different protein environments such as bovine serum albumin (BSA), human serum, and milk to test their stabilities. [Color figure can be viewed in the online issue, which is available at wileyonlinelibrary.com.]

All details involving the synthesis of the nanoparticle with varying concentration were provided in the Supporting Information section (Supporting Information Tables S1 and S2, Figs. S7 and S8). Nanoparticles with average size 56 nm have been selected to be used throughout of this article with the final polymer concentration of 0.5 mg/mL (in water). Figure 2 shows SEM (a), TEM (b) microscope images and DLS (c), zeta potential (d) histograms of NP-P1 with average size 56 nm.

In order to test the stability of P1NPs in water and PBS buffer (at pH 7.4), DLS measurements were taken over 35 days. The measurement results clearly show that there are no significant changes in the initial size of the nanoparticles confirming that these nanoparticles are stable in water and PBS buffer for prolonged time (Supporting Information Fig. S9).

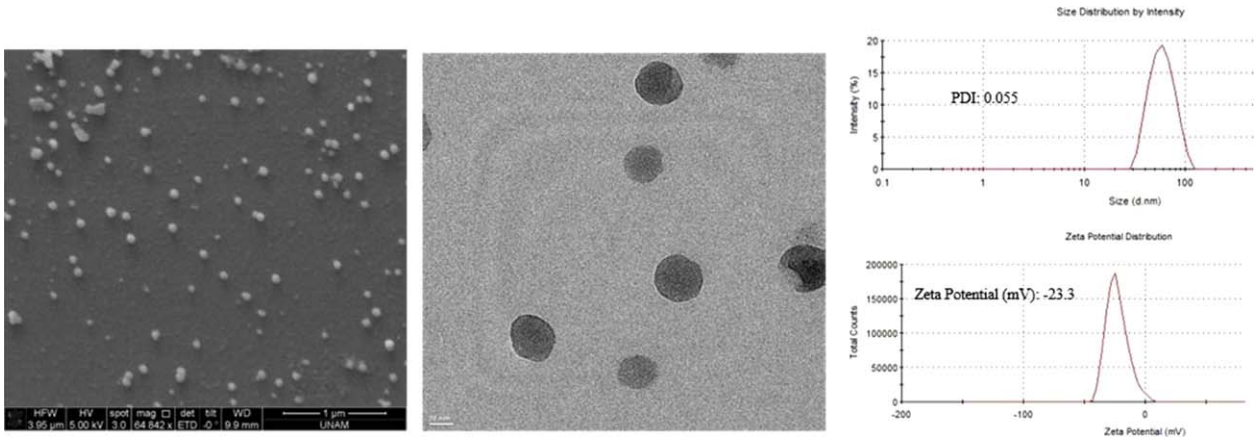

FIGURE 2 SEM (a), TEM (b) microscope images and DLS, zeta potential histograms of NP-P1. [Color figure can be viewed in the online issue, which is available at wileyonlinelibrary.com.]

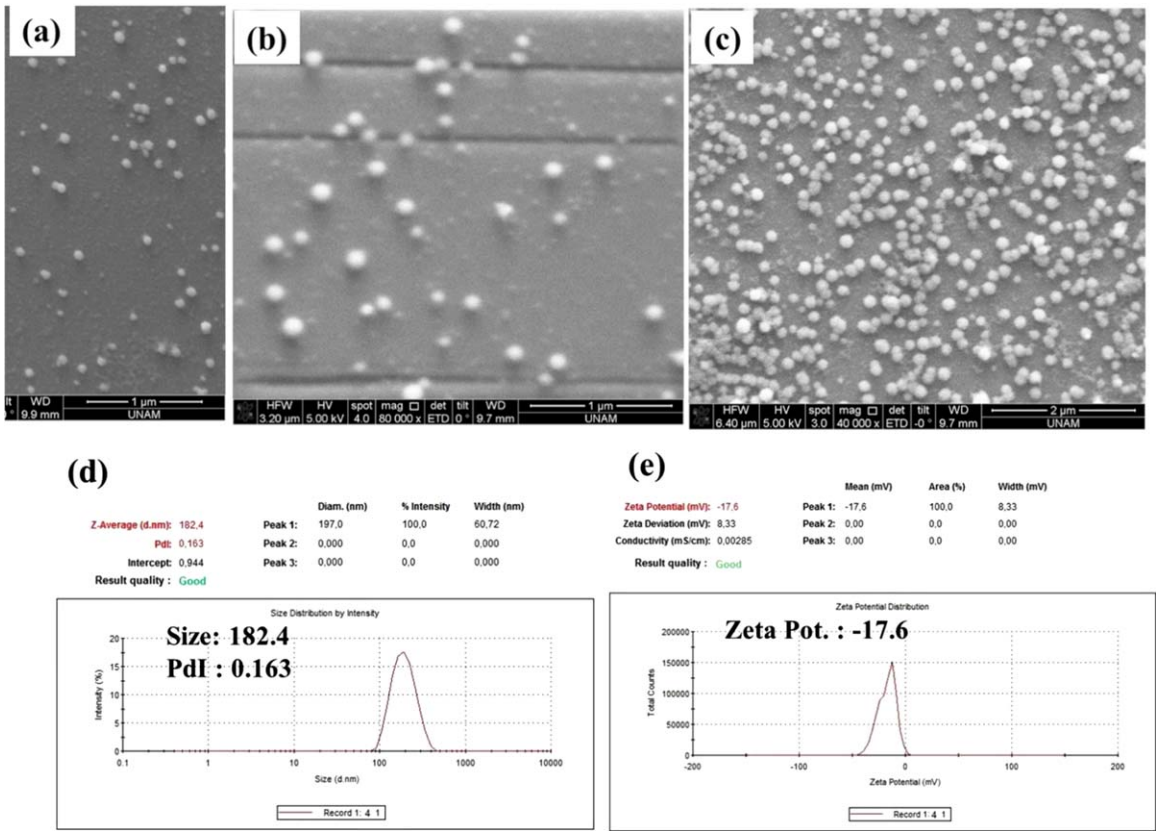

FIGURE 4 SEM images of NP-P1, (a) initial state (scale 1 μm), (b) after 4 h exposure of pH 5 (scale 1 μm), (c) after 4 h exposure of pH 5 (scale 2 μm), (d) DLS, zeta potential histograms of NP-P1 after 4 h exposure of pH 5. [Color figure can be viewed in the online issue, which is available at wileyonlinelibrary.com.]

Next, we incubated P1NPs in different protein environments such as bovine serum albumin (BSA), milk, and human serum to test their stabilities. The changes in the size of nanoparticles are insignificant in both BSA and milk media (Fig. 3). But there is around 10 nm increase in the incubation with human serum. This may be due to weak nonspecific interactions of nanoparticles with some of the proteins in the mixture.

The nanoparticles were further exposed to buffered aqueous solutions of pH 5.0 or 8.0 and their average sizes and zeta potential values were recorded at regular intervals (Supporting Information Figs. S10–S12). The size of the nanoparticles exposed to pH 5.0, was gradually increased from the initial size of 56 nm to 180 nm around 4 h and not much change was observed even after 24 h. The initial zeta potential value of −23 changed to −18 mV. SEM image of the nanoparticles showed the presence of spherical nanoparticles with about 180 nm average size (Fig. 4). Similar results were obtained with nanoparticles exposed to pH 8; however, in this case the initial size of nanoparticles increased from 56 nm to over 200 nm even in 1 h with zeta potential value of −24 (Supporting Information Fig. S12).

Although P1 is not a conventional pH-sensitive polymer which contain carboxylic or amine groups, still the size changes in the nanoparticles can be explained by the pH responsiveness of the polymer 1. P1 contains acetyl groups which can be hydrolyzed by acid or base. Consequently, the nature of the polymer could be switched from hydrophobic to hydrophilic by hydrolyzing acetyl group to hydroxyl group. In this way, nanoparticles made from acetyl group carrying polymer will exhibit hydrophobic character and have a rather compact shape, however, by the hydrolysis of acetyl groups to hydroxyl groups polymer chains will be loosely held because of the interaction of hydroxyl groups with water and the nanoparticles become larger.

Similar approach was reported by Griset et al.[44,45] In their work, first hydroxyl groups of the polymer used were protected as acetal to obtain a hydrophobic polymer which was utilized to prepare cross-linked nanoparticles. When these nanoparticles were exposed to pH 5, acetal groups were hydrolyzed to reveal hydroxyl groups and because of the interaction of hydroxyl groups with water the nanoparticles expanded 3 to 10 folds of their initial size. Although in our case the nanoparticles were not cross-linked, still they were not completely disintegrated into polymer chains after the hydrolysis due to the presence of a large hydrophobic polymer backbone which helps keeping them intact.

The faster size increase in shorter duration at pH 8, compared with pH 5 indicates that acetyl groups are hydrolyzed faster at pH 8 than pH 5. To prove further hydrolysis is

TABLE 1 Optical Properties of Polymer in Different Solvents, Dispersion of Polymer Nanoparticles in Water, in Acetate Buffer (pH 5.0), and Polymer Film

Solvent	λ_{abs} (nm)	λ_{em} (nm)	Φ_f[a] (%)	ε[b] (cm^{-1} M^{-1})
Chloroform	505	620	47.4	25,878
THF	510	627	31.9	21,813
DMF	515	640, 700 (sh)	17.3	12,119
Water	530	717	2.3	6902
Acetate buffer	530	717	3.0	7243
In film	544	731	n.d.	n.d.

[a] Fluorescent quantum yields are calculated using Rhodamine B in ethanol as standard (Φ_f: 98%).
[b] Molar absorptivity per repeat unit.
n.d.: not determined; sh: shoulder.

taking place, pH 5 and pH 8 treated nanoparticle dispersions were centrifuged to obtain precipitate which was redispersed in water and centrifugation was repeated to remove buffer residues. The collected precipitate was characterized by FT-IR spectrometer. FT-IR spectra of both samples show that the peak around 1700 cm^{-1} due to the carbonyl stretching of acetyl groups has disappeared indicating the hydrolysis of acetyl groups (Supporting Information Fig. S13).

Optical Properties of Polymer P1 and Nanoparticles

The optical properties of the nanoparticles were investigated by UV-Vis and fluorescence spectroscopy and compared with the polymers in different solvents and film; the results are tabulated in the Table 1.

Bathochromic shifts were observed in the absorption and emission spectra of the polymer P1 upon increasing the polarity of solvent (Supporting Information, Fig. S14) implying that the polymer has solvatochromic properties.[46] However, upon converting the polymer into nanoparticles larger bathochromic shifts are observed in the emission peaks which show similarities with the absorption and emission spectra of the polymer in film (the spectrum is provided in Supporting Information, Fig. S15). This suggests that the bathochromic shifts are not only due to solvent effect but also due to the intra and intermolecular interactions of polymer chains caused by tight folding.

Drug Loading Study of Polymer Nanoparticles

Camptothecin-loaded nanoparticles have been prepared in a single step synthesis. Briefly, polymers and CPT are dissolved in THF and injected into water while stirring under sonication. After the removal of THF, the dispersion of nanoparticles in water is obtained. In order to determine the loading and entrapment efficiency of the nanoparticles, ratios of CPT to polymers (w/w) 1:0.5, 1:1, 1:2, 1:6.25, 1:12.5, and 1:25 were used during the nanoparticle preparation. In each case, after the nanoparticle formation, the dispersion was dialyzed against water using a 14 kDa MWCO regenerated cellulose membrane for 24 h to remove any remaining unencapsulated CPT. The dialysates were analyzed by recording their absorption spectra ($\lambda_{max} = 366$ nm) and the unencapsulated CPT concentration was calculated from a calibration curve of CPT plotted from known concentrations of CPT solutions. The lowest detectable concentration in water was 25.4 nM which shows that our method allows us to detect less than 8% of CPT in the set with the lowest CPT concentration. The measurements taken from the dialysate of free CPT showed the same absorbance with the corresponding concentration of CPT suspension in water containing Tween 20 (0.2%, v/v) 24 h later. This shows that a 24 h-period is long enough for unentrapped CPT to homogenously disperse into medium. The entrapment efficiency (EE) and loading efficiency (LE) were calculated according to the following equations and the results are presented in Figure 5.

$$EE = \text{loaded drug wt.}/\text{total drug wt.} \times 100$$

$$LE = \text{loaded drug wt.}/\text{total system wt.} \times 100$$

The set with the lowest CPT concentration (drug:polymer ratio of 1:25) shows a 40% entrapment rate with the loading efficiency of 1.6%. As CPT concentration increases, loading efficiency increases up to around 9.8% and entrapment efficiency reaches a plateau value of 63% at the drug to polymer ratio of 1:6.25.

The synthesis of CPT-loaded CPNs was repeated more than three times by keeping the synthetic conditions constant. Their size was determined by dynamic light scattering (DLS) measurements and the results are tabulated in the Supporting Information Table S5. As it can be seen from the DLS measurements, the size of the drug loaded nanoparticles are dependent on the drug loading contents as there is a linear increase in the size of nanoparticles with increasing drug contents. However, the changes are not huge indicating that the structural integrity of the nanoparticles is not affected when they are loaded with drug. The reason could also be attributed to the π-π interactions between the aromatic conjugated backbone of the polymer chains and the aromatic rings of the CPT molecules, causing a close packing of the drug molecules.[37]

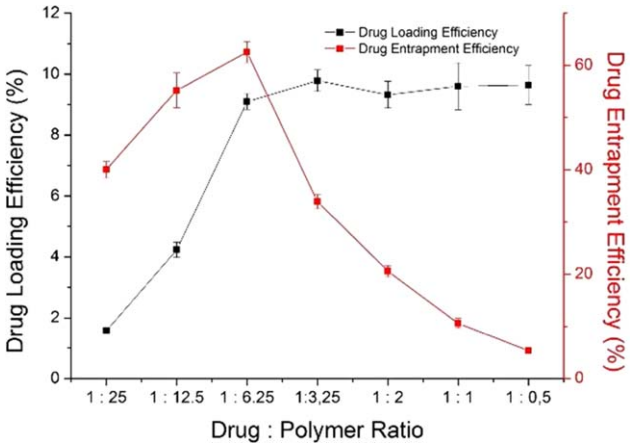

FIGURE 5 Drug loading and entrapment efficiencies. [Color figure can be viewed in the online issue, which is available at wileyonlinelibrary.com.]

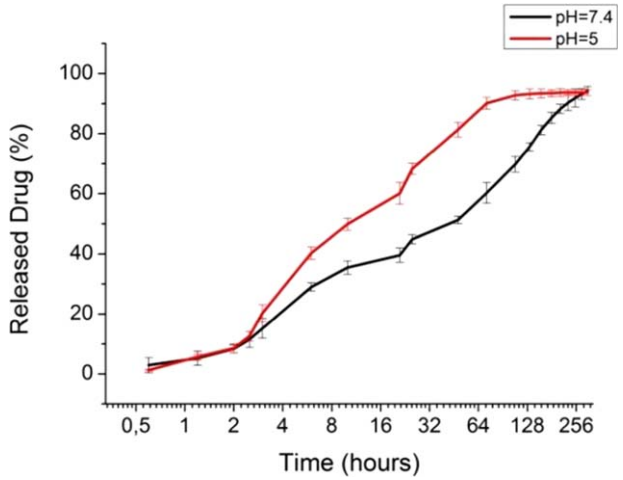

FIGURE 6 Percentage of cumulative release of CPT from NP1 at different pH. The release of drug molecules was monitored using a UV-Vis spectrophotometer (1:10 loading ratio of CPT/P1NP). [Color figure can be viewed in the online issue, which is available at wileyonlinelibrary.com.]

In Vitro Drug Release Study of Nanoparticles

The *in vitro* drug release studies of the nanoparticles with two different CPT contents as the CPT to P1NP ratios of 1:23 and 1:10 (determined after dialysis) were carried out at 37 °C at pH 5.0 (acetate buffer) and pH 7.4 (PBS). The time-dependent release profiles of CPT from the nanoparticles were measured by the absorption at 366 nm with UV-Vis spectrophotometry. Figure 6 shows the release profile of CPT loaded P1NPs (CPT to P1NP ratio of 1:10).

In the case of nanoparticles with high drug loading content, around 50% of drugs were released from P1NPs at pH 5.0 in the initial 12 h, and the release was sustained over 110 h, however, 90% of drugs have already released during 64 h. On the other hand, the release was slower in pH 7.4 compared with pH 5.0. Only 50% of the drugs were released around 48 h and 90% drug release reached to 256 h. The release of drugs from nanoparticles with low drug loading content was observed to be slightly faster at both pHs than the former case (Supporting Information Fig. S18); the reason could be due to π-π intermolecular interactions between the CPT molecules in high loading of nanoparticles which prevents the release of drugs.

The *in vitro* release studies demonstrated that the release of CPTs from NP1 were pH-dependent such that significantly faster drug release at mildly acidic pH of 5.0 (90% during 64 h) compared with physiological pH 7.4 (90% during 256 h) was observed. The above results indicated NP1 are appropriate vehicles for pH-triggered release of anticancer drugs.

In Vitro Cell Assays

Time and dose dependent *in vitro* cytotoxicity tests of blank and CPT-loaded nanoparticles (P1NPs) were performed by real-time cell electronic sensing (RT-CES)[47,48] assay with hepatocellular carcinoma cells (Huh7) over the course of 144 h. RT-CES experiments involve using a gold plate and the system relies on electrical impedance cell sensors arrays embedded at the bottom of the plates. In this experiment we have tested the cytotoxicities of P1NPs as well as CPT-loaded nanoparticles in two different drug loading contents. These nanoparticles were abbreviated as P1NP-A-CPT and P1NP-B-CPT which denote 1:62 and 1:10.4 (after dialysis), CPT/NP ratios, respectively. Free CPT was used as a positive control and DMSO and blank P1NPs were used as negative controls to the CPT-loaded P1NPs. Figure 7 shows the RT-CES assay results after the incubation of Huh7 cells with CPT, P1NPs blank, P1NP-A-CPT and P1NP-B-CPT over 144 h incubation period. Full experimental results were given in the Supporting Information Figure S17 and Table S6.

Blank nanoparticles at high concentrations (24.8 and 12.8 μM) appear to cause some changes in the cell behavior after 24 h incubation, growth inhibition reach to plateau values of 38 and 20%, for the nanoparticle concentrations of 24.8 and 12.8 μM, respectively, at 72 h and then the inhibition rate decreases rapidly and the cells starts to be responsive again and proliferate. This behavior may suggest the complex, dynamic nature of the interaction between the cells and nanoparticles. This could also be explained by an incidental enzyme interaction in which the NPs could randomly bind on some proteins to inhibit their activities, however, the cell signaling pathways get involved at this stage by increasing the expression of proteins to compensate the initial inhibition. As a result, this will cause no serious harm to the cells to go to apoptosis but only a temporary inhibition in the cell growth process.

If we investigate the behaviors of CPT and CPT delivered by nanoparticles with different concentrations, CPT as we observed in our previous study,[37] becomes rapidly effective in the cell growth inhibition even at the lowest concentration (0.1 μM) and shorter time (48 h). However, in both concentrations the growth inhibition is slower than free CPT confirming the slow release feature of the nanoparticles supported by *in vitro* drug release studies in different pHs. The release is even much slower in the case of the nanoparticles having high drug loading contents. This result might be explained by strong interactions between CPT molecules and polymer chains because CPT molecules can interact with each other more freely due to presence of fewer polymer chains to interfere with this process. In lower loading rates, CPT molecules can be evenly distributed in the polymer matrix; not unlike dissolution. Upon cell internalization, these matrices interact with hydrophobic membrane structures (endosomes) and CPT molecules can easily diffuse into these membranes to show activity in the cell. However, higher CPT content can bring out the intrinsic solubility problem of hydrophobic drugs. CPT molecules can easily form highly stable aggregates via π-π stacking inside the sparsely packed matrix and their likelihood of interacting with cellular hydrophobic compartments drops drastically. Therefore they show little to no cellular activity for a long time after cell internalization.

CPT-loaded P1NPs were analyzed by fluorescence microscopy on Huh7 cells. The red emission of P1NPs is an evidence for

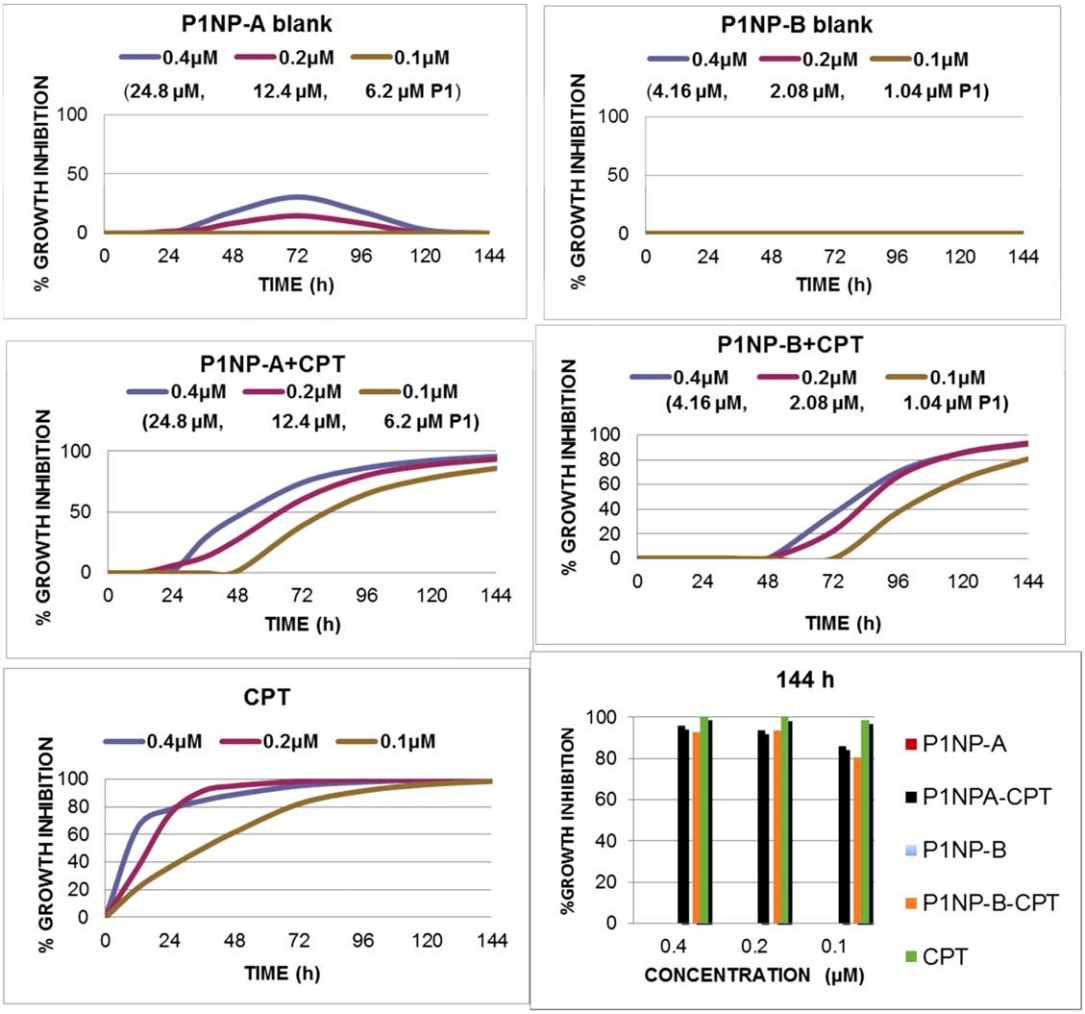

FIGURE 7 Real-time growth inhibitory effect of loaded and blank P1NPs with camptothecin on the human liver (Huh7) cancer cell line were determined by RT-CES. The full profiles of the CPT, P1NP, P1NP-A-CPT and P1NP-B-CPT exposed cells over 144 h duration. The concentrations are based on CPT concentrations but in brackets the concentrations of nanoparticles were also given. (0.1, 02, 04 μM CPT concentrations for 1:62 CPT/NP ratios correspond to 6.2, 12.4, 24.8 μM NP and for 1:10.4 CPT/NP ratios, 1.04, 2.08, 4.16 μM NP concentrations, respectively). The experiments were conducted in triplicate. [Color figure can be viewed in the online issue, which is available at wileyonlinelibrary.com.]

an efficient cellular internalization. Nuclei were stained with blue emitting Hoechst dye. The image of cells treated with P1NP-A-CPT (with CPT concentration of 0.1 μM) taken after 24 h incubation show the perinuclear accumulation of red-emitting nanoparticles (Supporting Information Fig. S21).

In the light of similar experiments in the literature[12,24–26] we suggest that NPs and the drug-loaded NPs might be internalized by cells through endocytosis and enriched in intracellular compartments, e.g., cytosolic vesicles and/or endosomes/lysosomes; however, further studies are needed for understanding whether they are differentially targeted into compartments.

CONCLUSIONS

We have reported the preparation of pH-sensitive, near-infrared emitting water dispersible conjugated polymer nanoparticles. The nanoparticle dispersions are stable in water over a month without forming any aggregates as well as stable in various biological media. These nanoparticles could be loaded with hydrophobic anticancer drugs with high loading efficiency for drug delivery and cellular imaging. The results indicate that these nanoparticles are promising as vehicles for image-guided, pH-triggered release of anticancer drugs. Currently the work regarding *in vivo* applications of this system is underway.

ACKNOWLEDGMENTS

We acknowledge TUBITAK-TBAG 112T704 and COST Action TD1004 (Theragnostics Imaging and Therapy: An Action to Develop Novel Nanosized Systems for Imaging-Guided Drug Delivery).

REFERENCES AND NOTES

1 K.Y. Choi, G. Liu, S. Lee, X. Chen, *Nanoscale* **2012**, *4*, 330–342.

2 J. Xie, S. Lee, X. Chen, X. *Adv. Drug Deliv. Rev.* **2010**, *62*, 1064–1079.

3 L. Chou, K. Ming, W. C. W. Chan, *Chem. Soc. Rev.* **2011**, *40*, 233–245.

4 Z. Cheng, A. Al Zaki, J. Z. Hui, V. R. Muzykantov, A. Tsourkas, *Science* **2012**, *338*, 903–910.

5 M. Elsabahy, K. L. Wooley, *Chem. Soc. Rev.* **2012**, *41*, 2545–2561.

6 C.-M. J. Hu, R. H. Fang, B. T. Luk, L. Zhang, *Nanoscale* **2014**, *6*, 65–75.

7 N. Kamaly, Z. Xiao, P. M. Valencia, A. F. R. Moreno, O. C. Farokhzad, *Chem. Soc. Rev.* **2012**, *41*, 2971–3010.

8 S. Nowag, R. Haag, *Angew. Chem. Int. Ed.* **2014**, *53*, 49–51.

9 S. Mura, J. Nicolas, P. Couvreur, *Nat. Mater.* **2013**, *12*, 991–1003.

10 G.-Y. Liu, L. Ping Lv, C.-J. Chen, X.-S. Liu, X.-F. Hu, J. Ji, *Soft Matter* **2011**, *7*, 6629.

11 W. Gao, J. M. Chan, O. C. Farokhzad, *Mol. Pharmaceutics* **2010**, *7*, 1913–1920.

12 J. R. Casey, S. Grinstein, J. Orlowski, *Nat. Rev. Mol. Cell. Biol.* **2010**, *11*, 50–61.

13 R. Alford, M. Ogawa, P. L. Choyke, H. Kobayashi, *Mol. Biol. Syst.* **2009**, *5*, 1279–1291.

14 Y. Wang, K. Zhou, G. Huang, C. Hensley, X. Huang, X. Ma, T. Zhao, B. D. Sumer, R. J. DeBerardinis, J. Gao, *Nat. Mater.* **2014**, *13*, 204–212.

15 J. A. Barreto, W. O'Malley, M. Kubeil, B. Graham, H. Stephan, L. Spiccia, *Adv. Mater.* **2011**, *23*, H18–H40.

16 B. N. G. Giepmans, S. R. Adams, M. H. Ellisman, R. Y. Tsien, *Science* **2006**, *312*, 217.

17 P. Zrazhevskiy, M. Sena, X. Gao, *Chem. Soc. Rev.* **2010**, *39*, 4326–4354.

18 Yan, J. L.; Estevez, M. C.; Smith, J. E.; Wang, K. M.; He, X. X.; Wang, L.; Tan, W. H. *Nano Today* **2007**, *2*, 44–50.

19 D. Tuncel, H. V. Demir, *Nanoscale* **2010**, *2*, 484–494.

20 I. O. Ozel, T. Ozel, H. V. Demir, D. Tuncel, *Opt. Express* **2010**, *18*, 670–684.

21 E. J. Park, T. Erdem, V. Ibrahimova, S. Nizamoglu, H. V. Demir, D. Tuncel, *ACS Nano* **2011**, *5*, 2483–2492.

22 V. Ibrahimova, S. Ekiz, O. Gezici, D. Tuncel, *Polym. Chem.* **2011**, *2*, 2818–2824.

23 J. Pecher, S. Mecking, *Chem. Rev.* **2010**, *110*, 6260–6279.

24 C. Wu, D. T. Chiu, *Angew. Chem. Int. Ed.* **2013**, *52*, 3086–3109.

25 N.A. A. Rahim, W. McDaniel, K. Bardon, S. Srinivasan, V. Vickerman, P. T. C. So, J.H. Moon, *Adv. Mater.* **2009**, *21*, 3492–3496.

26 P. Howes, R. Thorogate, M. Green, S. Jickells, B. Daniel, *Chem. Commun.* **2009**, 2490–2492.

27 A. Kaeser, A. P. H. J. Schenning, *Adv. Mater.* **2010**, *22*, 2985–2997.

28 I. Fischer, K. Petkau-Milroy, Y. L. Dorland, A. P. H. J. Schenning, L. Brunsveld, *Chem. Eur. J.* **2013**, *19*, 16646–16650.

29 P. Howes, M. Green, D. Parker, G. Varma, M. Kallumadil, M. Hughes, A. Warley, A. Brain, R. Botnar, *J. Am. Chem. Soc.* **2010**, *132*, 9833.

30 P. Howes, M. Green, J. Levitt, K. Suhling, M. Hughes, *J. Am. Chem. Soc.* **2010**, *132*, 3989.

31 K. Pu, A. J. Shuhendler, J. V. Jokerst, J. Mei, S. S. Gambhir, Z. Bao, J. Rao, *Nat. Nanotechnol.* **2014**, *9*, 233–239.

32 L. Feng, C. Zhu, H. Yuan, L. Liu, F. Lva, S. Wang, *Chem. Soc. Rev.* **2013**, *42*, 6620–6633.

33 C. F. Wu, S. J. Hansen, Q. O. Hou, J. B. Yu, M. Zeigler, Y. H. Jin, D. R. Burnham, J. McNeill, J. M. Olson, D. T. Chiu, *Angew. Chem. Int. Ed.* **2011**, *50*, 3430–3434.

34 X. Wang, F. He, L. Li, H. Wang, R. Yan, L. Li, *ACS Appl. Mater. Interfaces* **2013**, *5*, 5700−5708.

35 X. L. Feng, F. T. Lv, L. B. Liu, H. W. Tang, C. F. Xing, Q. O. Yang, S. Wang, *ACS Appl. Mater. Interfaces* **2010**, *2*, 2429–2435.

36 H. Gong, L. Cheng, J. Xiang, H. Xu, L. Feng, X. Shi, Z. Liu, *Adv. Funct. Mater.* **2013**, *23*, 6059–6067.

37 O. Gezici, I. Durmaz, E. Bilget Guven, O. Unal, A. Ozgun, R. Cetin-Atalay, D. Tuncel, *RSC Adv.* **2014**, *4*, 1302–1309.

38 S. Binauld, M. H. Stenzel, *Chem. Commun.* **2013**, *49*, 2082–2102.

39 A.W. Jackson, D. A. Fulton, *Polym. Chem.* **2013**, *4*, 31–45.

40 J. Pennakalathil, E. Jahja, E. S. Özdemir, Ö. Konu, D. Tuncel, *Biomacromolecules* **2014**, *15*, 3366−3374.

41 J. Geng, Z. Zhu, W. Qin, L. Ma, Y. Hu, G. G. Gurzadyan, B. Z. Tang, B. Liu, *Nanoscale* **2014**, *6*, 939.

42 J. Liu, G. Feng, D. Ding, B. Liu, *Polym. Chem.* **2013**, *4*, 4326–4334.

43 Z. Guo, S. Park, J. Yoon, I. Shin, *Chem. Soc. Rev.* **2014**, *43*, 16–29.

44 A. P. Griset, H. Colby, Y. L. Colson, M. W. Grinstaff, *Nanoscale* **2013**, *5*, 3496–3504.

45 A. P. Griset, J. Walpole, R. Liu, A. Gaffey, Y. L. Colson, M. W. Grinstaff, *J. Am. Chem. Soc.* **2009**, *131*, 2469–2471.

46 B. Valeur, Molecular Fluorescence: Principles and Applications; Wiley-VCH: Weinheim, **2002**.

47 L. Otero-Gonzalez, R. Sierra-Alvarez, S. Boitano, Jim A. Field, *Environ. Sci. Technol.* **2012**, *46*, 10271–10278.

48 K. Solly, X. B. Wang, X. Xu, B. Strulovici, W. Zheng, *Assay Drug Dev. Technol.* **2004**, *2*, 363–372.